Cooperativity and Coverage Dependent Molecular Desorption in Self-Assembled Monolayers: Computational Case Study with Coronene on Au(111) and HOPG

Received 00th January 20xx,
Accepted 00th January 20xx

DOI: 10.1039/x0xx00000x

Bhaskar Chilukuri,*[a] Ursula Mazur,[a] and K. W. Hipps*[a]

One of the common practices in the literature of molecular desorption is the comparison of theoretically (mostly using DFT) calculated single molecule adsorption energies with experimental desorption energies from studies like temperature programmed desorption (TPD) *etc*. Comparisons like those do not consider that the experimental desorption energies are obtained via ensemble techniques while theoretical values are calculated at the single molecule level. Theoretical values are generally based upon desorption of a single molecule from a clean surface, or upon desorption of an entire monolayer. On the other hand, coverage dependent molecule-molecule interactions add to and modify molecule-substrate interactions that contribute to the experimentally determined desorption energies. In this work, we explore the suitability of an additive nearest neighbor model for determining general coverage dependent single molecule desorption energies in non-covalent self-assembled monolayers (SAMs). These coverage dependent values serve as essential input to any model attempting to reproduce coverage dependent desorption or for understanding the time dependent desorption from a partially covered surface. This method is tested using a case study of coronene adsorbed on Au(111) and HOPG substrates with periodic DFT calculations. Calculations show that coronene exhibits coverage and substrate dependence in molecular desorption. We found that intermolecular contact energies in the coronene monolayer are not strongly influenced by the HOPG substrate, while coronene desorption on Au(111) exhibits strong cooperativity where the additive model fails.

Introduction

Surfaces functionalized by self-assembled monolayers[1] (SAM) have applications in molecular electronics,[2,3] catalysis,[4] corrosion control,[5] sensors,[6] *etc*. Hence, the kinetics and thermodynamics of these systems is of immense interest.[7,8,9-10] One of the important quantities needed to determine both equilibrium and kinetic processes on surfaces is the adsorption/desorption energy of molecules forming the adlayer. Adsorption and desorption of SAMs from the vapor are directed by adsorbate-substrate, adsorbate-adsorbate interactions.[11,] At the solution-solid (SS) interface solvent-substrate, solvent adlayer, and solvent-solute interactions also influence the self-assembly process. Molecular desorption involves the interplay of all the aforementioned chemical interactions.

Conventionally, desorption of SAMs is studied experimentally using temperature programmed desorption (TPD),[12-14] quartz crystal microbalance,[15-17] ellipsometry,[18,19] surface plasmon resonance,[20,21] harmonic generation,[22] chronoamperometry,[23] or a variety of spectroscopic techniques like IR,[24] XPS,[25] mass,[26] *etc*. But the desorption energies obtained through conventional techniques are at the ensemble level, where the energies obtained are averaged over a large number of molecules, adsorption sites and variable surface coverages. For example, desorption energies from TPD experiments are typically coverage dependent and most values reported in the literature includes a '*forced compensation effect*'[27,28] which can lead to false pre-exponential factors and activation energies and hence false desorption energies. Coverage dependent measurements have been reported[29,30] to provide a so called '*complete analysis*'[27,31] of TPD spectra. Yet, these measurements are at an ensemble level. Perhaps the most insightful computational study was that of Nieskens et al[27] who used Monte Carlo Modeling of a system with pair wise interactions to compute the TPD and then fit various models to that data. They found that a coverage dependent contribution could be extracted from the adsorption energy provided their proposed analysis method was used. Even in this case, however, the molecular interactions are not resolved, just their overall effect on the macroscopic surface.

Scanning probe microscopy (SPM), is a technique available to study surface desorption characteristics of single molecules.[7,8,32] Recently Hipps et al. reviewed measurement of desorption rates of non-covalent SAMs at the SS-interface.[33] In the review, a typical potential energy surface (PES) of single molecule desorption is presented for a monocomponent network with single morphology. Unlike the PES in surface chemistry and catalysis[34,35,36] which involves a reaction coordinate with

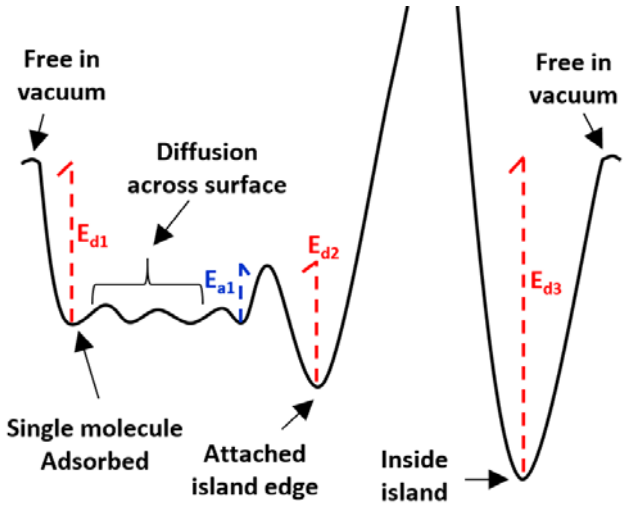

Fig. 1 Potential energy surface of a single molecule as it moves from vacuum to a solid substrate. The red dotted lines represent desorption energies and blue dotted line represents adsorption energy.

[a] *Department of Chemistry, Washington State University, Pullman, WA 99164-4630, USA.*

† Footnotes relating to the title and/or authors should appear here.
Electronic Supplementary Information (ESI) available: [details of any supplementary information available should be included here]. See DOI: 10.1039/x0xx00000x

bond making and bond breaking, the PES in non-covalent SAMs involves physisorption, diffusion and desorption, mostly through van der Waals interactions. Based on PES of molecular desorption at SS-interface,[33] a similar PES for molecular desorption at the vacuum-solid interface is shown in Fig. 1. In this PES, a single molecule in vacuum adsorbs onto a substrate from which the desorption energy is E_{d1}. Once the molecule is on the surface, it can diffuse across the surface and reach an edge of an island of an ordered network with an adsorption energy of E_{a1}. If the molecule must move from the edge of the island to being free on the surface, it requires a desorption activation energy of E_{d2}. Therefore, for a molecule to desorb from the edge of the island to vacuum, the desorption energy is $E_{d2}+E_{d1}-E_{a1}$. On the other hand, if the molecule must desorb from the inside of an island to vacuum, the desorption energy is E_{d3}. To complicate the issue, the details of the number (and possibly orientation) of molecules initially adjacent to the desorbing molecule will affect the desorption energy. Similarly, the location of an edge molecule (number of contacts) will affect the activation energy E_{d2}. Obtaining all the adsorption/desorption and activation energies implied by Fig. 1, using SPM is hard even for a monocomponent system with single morphology while in fact, an actual SAM can have multiple grain boundaries, step edges and morphologies. Also, it is possible to have a multicomponenet network where the PES can be more complicated than Fig. 1.

In this work, we present a ***simple model to determine the single molecule desorption energy of a specific molecule in a physisorbed non-covalent SAM*** at the vacuum-solid interface using density functional theory (DFT) calculations. Most theoretical studies in the literature[37- 44] usually calculate the adsorption energy of an isolated molecule where the calculated energy is only dominated by the molecule-substrate interactions. As one can see from Fig. 1, single molecule desorption energy varies based on the surface coverage. In other words, desorption energy is dependent upon the number of nearest neighbor molecules surrounding a specific adsorbate. While the desorption energy is also dependent upon the adsorption site relative to the substrate, in this study we restrict consideration to the site occupied by the optimized monolayer. Unlike earlier studies,[40-44] here we use a combination of molecule-substrate binding energy and molecule-molecule contact energies to determine single molecule desorption energy. ***Our goal here is to determine the role and contribution of intermolecular contact energies to single molecule desorption energy from substrates***. As representative systems, we choose a monocomponent network of coronene molecules adsorbed on Au(111) and HOPG substrates with single morphology to determine the desorption energies. This model is the one used by Nieskens et al.[27] for the coverage dependent desorption energy, but they used an empirical parameter while we actually calculate the values here. We note that this model assumes all clusters of coronene on the surface have the same structure as the experimental equilibrium structure. We realize this is a simplification that could be accounted for by including more representative systems. Doing so, however, would not affect the primary purpose of this study – to show that the use of a single surface configuration for calculation of desorption energies is not realistic.

Models and Methodology

Geometries for DFT calculations

Different geometries of coronene on Au(111) and HOPG for DFT calculations were developed using previously reported surface lattice structures from scanning tunneling microscopy (STM) experiments. Jahanbekam *et al.*,[45] have shown that coronene can have multiple polymorphs on Au(111), but here we only consider the high-density surface structure for our calculations. The high-density epitaxial coronene/Au(111) lattice structure has a hexagonal symmetry with intermolecular spacing of 1.15 ± 0.04 nm. This structure also matches with other STM studies of coronene/Au(111).[46-48] Walzer et al.[49] reported the first STM study of coronene/HOPG interface which had a six-fold symmetrical lattice with intermolecular spacing of 1.11 ± 0.01 nm. This structure also matches with other STM studies of coronene/HOPG.[30,50] We use Jahanbekam's[45] and Walzer's[49] surface structures of coronene on Au(111) and HOPG respectively to develop our computational geometries.

It is important to note that experimental STM sturctures show coronene binds epitaxially to Au(111)[45] and HOPG[49] with one coronene molecule per lattice. Using the step edge and the reconstruction lines on Au(111), Jahanbekam et al., determined the orientation of coronene molecules on Au(111) which has head-to-head coronene hydrogens configuration with its nearest neighbor. On the other hand, Thrower et al., showed that coronene molecules adsorb in a staggered configuration on HOPG.[30] Hence, we used head-to-head and staggered coronene orientations on Au(111) and HOPG respectively for our computational modeling. Furthermore, these configurations are determined to be lowest energy configurations based on preliminary periodic DFT calculations (Section S1, Fig. S1 in supplementary information). For developing our computational geometries, we use 4x4 supercells of the optimized head-to-head configuration of coronene/Au(111) (Fig. S1-B) and staggered configuration of coronene/HOPG (Fig. S1-C). The corresponding initial (before optimization) geometries of monolayer of coronene on Au(111) and HOPG are shown in Figures S2 and S3 respectively.

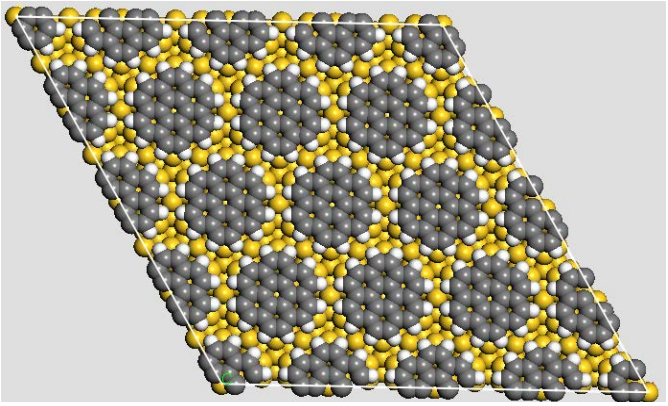

Fig. 2 Geometry of coronene/substrate (substrate = Au(111) or HOPG. Colors: Substrate-yellow, grey-coronene and white line represents hexagonal lattice.

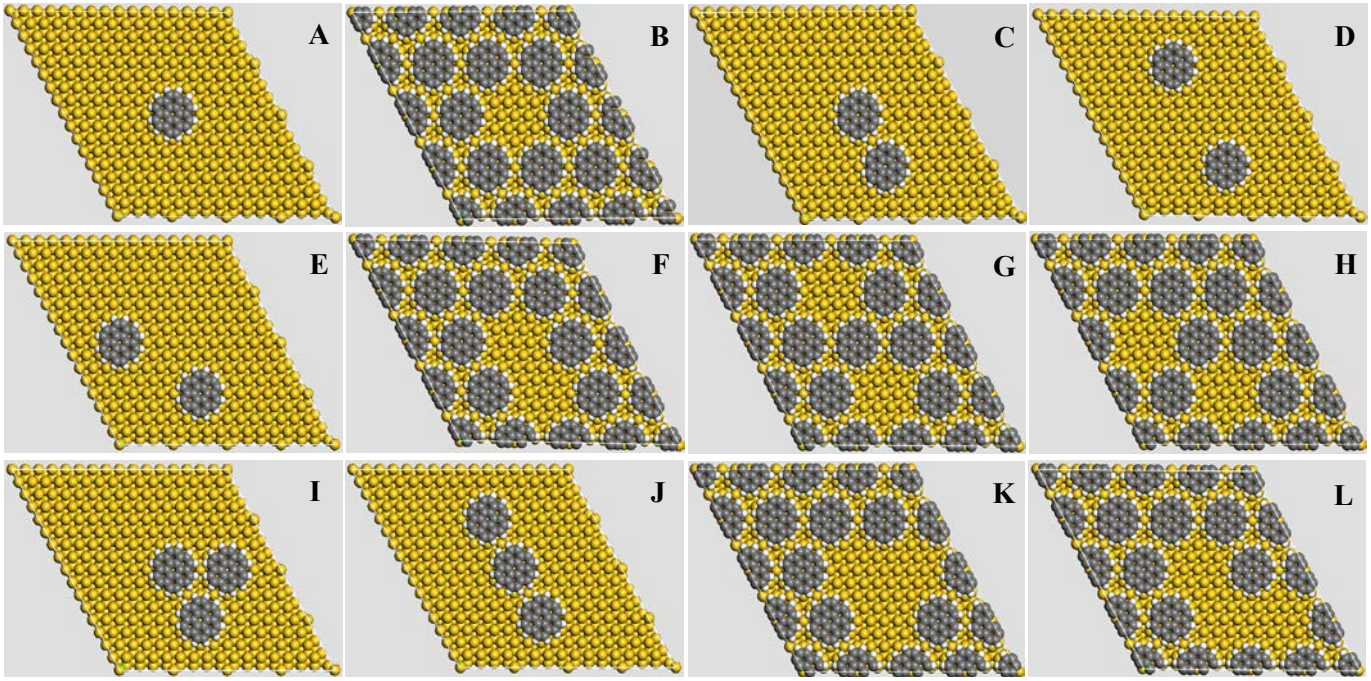

Fig. 3 Geometries of coronene/substrate (substrate = Au(111) or HOPG with variable surface coverage. Colors: Substrate-yellow, grey-coronene. Note that A, C, D, E, I, and J represent the situation before desorption with a final state of all molecules desorbed, while the others represent an initial monolayer with the final desorbed state shown.

For simplicity, we present Fig. 2 which represents a typical geometry (irrelevant of coronene orientation) of coronene/substrate (substrate = Au(111), HOPG) system based on 4x4 supercell of the respective STM lattice structures.[45,49] This geometry is a hexagonal lattice with 16 coronene molecules in the lattice representing complete surface coverage. The Au(111) substrate has 3 layers of gold, while the HOPG substrate has 2 layers of carbon. The lattice parameters for the coronene/Au(111) system are a = b = 46.14 Å and α = β = 90º, γ = 120º with intermolecular coronene separation of 11.54 Å. For the coronene/HOPG system, the lattice parameters are a = b = 45.02 Å and α = β = 90º, γ = 120º with intermolecular coronene separation of 11.26 Å. This indicates that coronene molecules are packed more tightly by ~0.28 Å on HOPG than on Au(111). The coronene/substrate lattice parameters (Fig. 2, 3) match the experimental STM structures of Jahanbekam[45] and Walzer.[49] The coronene/substrate geometries are fully relaxed with various DFT functionals (*vide infra*) before any further analysis.

Using Fig. 2 as a template, multiple periodic geometries with variable surface coverage were developed as shown in Fig. 3. The variation in surface coverage in all the geometries in Fig. 3 is reminiscent of different locations on the PES in Fig. 1. For example, Fig. 3A represents an isolated molecule adsorbed onto the substrate, while Fig. 3B represents a monolayer from which a single molecule is desorbed from the inside of an island. Fig. 3F-3H also represents molecules desorbed from inside of an island but with variable neighboring contacts. Fig.-3C,3D,3E,3I,3J represents two or three molecules on the substrate with variable intermolecular distances while Fig.-3K,3L represent molecules desorbing from the edge of the island. *Two important variables should be noticed in all the geometries in Fig. 3. First, the number of contacts lost for each desorbing molecule and second the intermolecular separation between the molecules in each geometry. Using the geometries in Fig. 3, we will determine desorption energies that vary with intermolecular contacts and molecule-substrate binding*. Note that Fig.3 represent typical models derived from Fig. 2 irrespective of the orientation of coronene molecules on substrate. As we have mentioned earlier if the substrate is Au(111), the coronene orientation is head-to-head (Figure S2), and if the substrate is HOPG, the coronene orientation is staggered (Figure S3) with respect to its neighbor. So, DFT optimizations performed on each model (Fig. 3) represent each of the respective coronene orientation on the corresponding substrate.

Computational Methods

Periodic DFT calculations were performed using VASP[51,52] on all the models in Fig. 2 and 3 and on clean substrates and on the isolated coronene molecule. For all slab calculations a vacuum layer of 12 Å is used in the z-axis. Periodic calculations were performed using plane-wave density functional theory (PW-DFT) within the projector augmented wave (PAW) method[53,54] to describe the core electrons and valence–core interactions. All calculations were performed with dispersion corrected vdW-DF[55] functional of Klimes which is based on work by Langreth and Lundqvist *et al.*[56] which considers the nonlocal nature of electron correlation. We used two different vdW-DF GGA functionals, the optB88-vdW and the optB86b-vdW with PAW potentials optimized for the PBE functional having *p*, *s* semicore valence for Au atoms. It was previously reported[57,58,59] that calculations with dispersion corrected vdW-DF functional yields better geometries and properties in contrast to experiment than with conventional hybrid DFT functionals. For all calculations, the electronic wave functions are sampled in a *k*-point grid of 1×1×1 in the irreducible Brillouin zone (BZ) using the Monkhorst and Pack (MP)[60] method. A plane wave cut off

Table 1. Parameters used in least squares fit analysis. Geometries listed in the table refers to Figure 3.

Geometry ID (i)	Desorbed Molecules (n_i)	Lost Contacts (c_i)
A	1	0
B	1	6
C	2	1
D	2	0
E	2	0
F	2	11
G	2	12
H	2	12
I	3	3
J	3	2
K	3	15
L	3	16

energy of 550 eV was used for all simulations which is chosen based on the energy convergence of primitive lattice structures of Au(111), HOPG and isolated coronene molecule. Methfessel–Paxton smearing was used to set the partial occupancies for each wave function with a smearing width of 0.2 eV. All the geometries were fully optimized up to ~0.001 eV energy convergence with both optB88-vdW and optB86b-vdW functionals, while keeping the bottom layer of the substrate constant in each coronene/substrate (substrate = Au(111), HOPG) system. Hence for each coronene/substrate system, a total of 15 calculations with each functional yields a total of 60 DFT optimized systems.

Results and Discussion

Upon optimizing all the geometries in Fig. 3, the desorption energy (E_i) of a coronene molecule in any given geometry 'i' is fitted to the following nearest neighbor interaction energy model,

$$E_i = E_0 \mp a \cdot \sum_{kj} \delta_{kj} \qquad (1)$$

where, E_0 = best fit desorption energy of single isolated coronene molecule on the substrate, δ_{kj} = 1 if each missing molecule 'k' has a nearest neighbor 'j' and 'a' = average coronene-coronene contact energy which is a fitting parameter. The parameter 'a' is equivalent to ω^{NN} in reference 27, except they parameterized for 4 nearest neighbors while we have 6. The parameter 'a' is determined from the following least squares fitting (LSF) equations, where we minimize the difference between the DFT calculated energy associated with a given geometry (E_i) and the energy calculated from the nearest neighbor interaction model eq 1.

$$F(a)_i = E_i - (n_i E_0 + a c_i) \qquad (2)$$

$$X(a) = \sum_i (F(a)_i)^2 \qquad (3)$$

where, n_i = number of desorbed molecules in geometry 'i', and c_i = total number of contacts lost in each geometry. $F(a)_i$ is the total error in desorption energy for each different geometry, 'i', shown in Fig. 3. X(a) is the sum of the squares of error $F(a)_i$ from which 'a' is obtained. Table 1 shows the number of desorbed molecules (n_i) and total lost contacts (c_i) for each geometry, 'i'.

Table 2. Parameters obtained from PW-DFT and least squares fitting calculations. E_0 is best fit desorption energy of single isolated coronene on substrate. 'a' is the average contact energy between coronenes. E_d is the calculated desorption energy of an isolated coronene on a given substrate.

Coronene/ Substrate System	vdW-DFT Functional	E_0 (eV)	'a' (meV)	E_d (eV)
Coronene/HOPG	optB88	2.11	58	2.12
Coronene/HOPG	optB86b	2.12	52	2.13
Coronene/Au(111)	optB88	2.08	55	2.06
Coronene/Au(111)	optB86b	2.39	-3	2.38
Coronene/Au(111)	optPBE	2.06	78	2.09
Coronene ML only from HOPG	optB88	0.01	54	-
Coronene ML only from HOPG	optB86b	0.00	54	-
Coronene ML only from Au(111)	optB88	0.00	40	-
Coronene ML only from Au(111)	optB86b	-0.01	40	-
Coronene ML only from Au(111)	optPBE	0.00	64	-

The corresponding E_0 and 'a' values obtained form LSF for coronene/substrate systems using optB88 and optB86b vdW-DF functionals are listed in Table 2.

To determine the role of substrates on the intermolecular contact energies ('a'), we performed similar PW-DFT calculations and LSF analysis on *coronene only geometries without the substrate*. For these calculations the substrates were removed and the geometries of the coronene only monolayers (ML) were kept intact and single point energies were determined. We refer to these geometries as "coronene ML only" systems (Table 2). Using the single point energies, analysis was carried out using equations 1-3 for all "coronene ML only" systems from HOPG and Au(111) and corresponding E_0 and 'a' are listed in Table 2. Additionally, desorption energies (E_d) (obtained using equation-S1,S2 in supplementary information) of isolated coronene molecule on HOPG and Au(111) substrates were also listed in Table-2. The calculated E_d values listed in Table 2 are consistent with reported experimental and theoretical desorption energies of coronene on HOPG.[30] E_d of coronene on Au(111) from experiment is not reported to the best of our knowledge. We attempted TPD experiments for coronene on Au(111) and found that the coronene monolayer does not completely desorb from gold. Based on the work by Talyzin et. al.,[61] we think that coronene may have turned to graphene like structures on Au(111) at high temperatures. But, the calculated E_d of coronene on Au(111) (Table-2) matches with other DFT calculations in the literature.[62,9]

Fig. 4 shows total error, $F(a)_i$, in calculated desorption energy between the DFT results and the nearest neighbor model. Model energies were based on fitted contact energies, 'a' for each geometry, 'i' (Table 2). The $F(a)_i$ values range within 20 meV for coronene on HOPG with both DFT functionals, while the errors range from 50-150 meV for coronene on Au(111). Also the 'a' values are 58 and 52 meV (Table 2) for coronene/HOPG systems while they change to 55 meV for

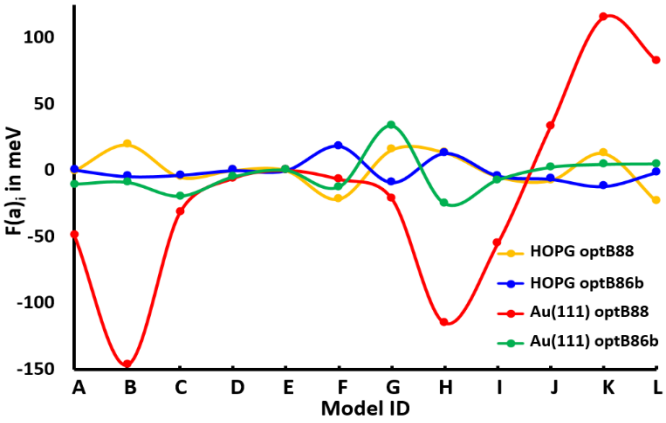

Figure 4. Errors, $F(a)_i$, in energy for each geometry (see Figure 3) of coronene/substrate (where, substrate = HOPG (orange, blue) or Gold (red, green) with optB88 and optB86b vdW-DF functionals. The error fluctuation (y-axis) in each plot is relative to energy (E_0) of single isolated coronene molecule on substrate. Note that relatively weak error fluctuation of optB86b-vdW functional (green) on Au(111) is due near zero interaction energy (*vide supra and Table 2*). The line connecting points is solely meant to guide the eye.

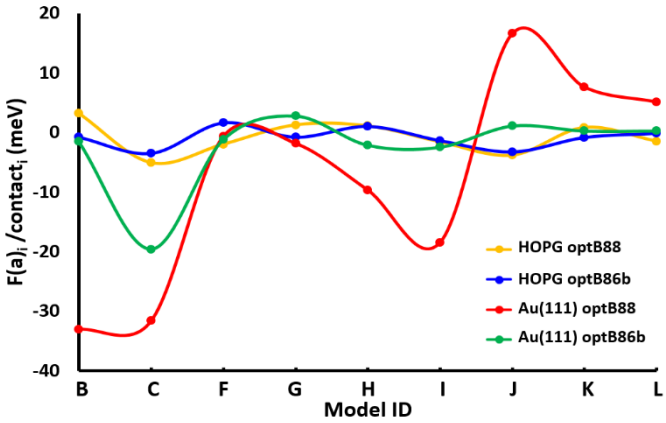

Figure 5. Errors per contact, $F(a)_i/c_i$, for geometries with contacts (see Figure 3) of coronene/substrate (where, substrate = HOPG (orange, blue) or Gold (red, green) with optB88 and optB86b vdW-DF functionals. The error fluctuation (y-axis) in each plot is relative to energy (E_0) of single isolated coronene molecule on substrate. Note that relatively weak error fluctuation of optB86b-vdW functional (green) on Au(111) is due near zero interaction energy (*vide supra and Table 2*). The line connecting points is solely meant to guide the eye.

coronene/Au(111) system with optB88-vdW . Note that all these 'a' values are positive which are indicative of attractive interaction/contact energies. The optB86b-vdW functional gave only -3 meV (repulsive energy) for the coronene/Au(111) system. That is, optB86b-vdW predicted slightly repulsive interaction between coronenes on Au(111). This is the origin for what appear to be very good fits in Figures 4 and 5. This could be due to the interplay of stabilizing and destabilizing interactions of each coronene molecule with the gold substrate and with its neighbors when optB86b-vdW functional is used.[63] Similar observations for other physisorbed systems on metals have been reported.[63-65] Gautier et. al.,[63] have noted that there is no universal DFT functional that yields correct energies all the time and hence a combination of DFT functionals have to be checked to determine a trend. Due to significant differences in $F(a)_i$ and 'a' values for coronene/Au(111) systems with optB88 and optB86b vdW-DF functionals, we performed an additional set of calculations with optPBE vdW-DF functional[55,56,66] on all coronene/Au(111) geometries (Fig. 2 and 3) followed by fitting the data to our model. The corresponding $F(a)_i$ and 'a' value are shown in section-S3 and Fig. S4, S5 in the supplementary information. Coronene-coronene contact energies 'a' with optPBE-vdW functional are determined to be 78 and 64 meV with and without the Au(111) substrate (Table 2). These values are consistent with calculated values of coronene/Au(111) systems with optB88-vdW functional (Table 2) indicating that optB86b-vdW functional underestimates 'a' in the presence of a Au(111) substrate. Calculations with various functionals (Table 2) show that coronene-coronene contact energies for various geometries (Fig. 3) fluctuate less (~20 meV) when coronene is bound to HOPG. In contrast, coronene-coronene contact energies vary significantly (50-150 meV) when coronene is bound to Au(111). These results indicate that there may be a high degree of cooperative binding in coronene/Au(111) systems, where the site of desorption (like the edge of island or inside of island, see Fig. 1 and 3) plays an important role in the contact energies unlike the coronene/HOPG systems where the error, $F(a)_i$ is less than 25 meV (Fig. 4) regardless of the adsorption location.

Note that the data shown in Fig. 4 are total errors in desorption energy for each geometry. As one can see from Table 2, the number of lost contacts and molecules desorbed vary from geometry to geometry. To determine if the number of lost contacts in each geometry is influencing the total error fluctuation in Fig. 4, we divided the total error, $F(a)_i$, with the number of lost contacts (c_i) and replotted them in Fig. 5. If the geometries do not have any lost contacts (geometries 3A, 3D, 3E), then they are not shown in Fig. 5. The magnitude of errors has now been lowered significantly compared to Fig. 4. For coronene/HOPG systems the error per contact ranges within 5 meV while the coronene/Au(111) systems the error ranges within 30 meV. Thus, the model "error" is less than 10% for the case of coronene on HOPG but can be as large as 50% for coronene on gold.

As we discussed in Fig. 1, single molecule desorption in SAMs may be a multistep process which depends on the location of desorption. For example, if coronene molecules must desorb like 'Geometry K' (Fig. 3K), a total of 3 molecules must desorb (Table 1). The first coronene molecule desorbing has 6 neighboring contacts, the second molecule adjacent to it has 5 contacts and the third molecule has 4 contacts, giving a total of 15 lost contacts (Table 1). If the DFT functional used is optB88-vdW and substrate is HOPG, the first desorbing molecule should have a total desorption energy ($E_{d\text{-}Total}$) which is the sum of desorption energy of isolated coronene molecule on HOPG, E_d (2.12 eV, Table 2) and six times the coronene-coronene contact energy, 6*'a' = (6*(58 meV) = 348 meV (Table 2). Since the error per contact, $F(a)_i/c_i$, for coronene/HOPG ranges within 5 meV (6*5 meV = 30 meV) (Fig. 5), the total desorption energy ($E_{d\text{-}Total}$) for first desorbing molecule in 'Geometry K' (Fig. 3K) should at least be 2.12 eV + 348 meV ± 30 meV = 2.47 ± 0.03 eV. Consequently, $E_{d\text{-}Total}$ for second desorbing molecule should be E_d+5*'a' = 2.41 ± 0.02 eV and $E_{d\text{-}Total}$ for the third desorbing molecule is E_d+4*'a' = 2.35 ± 0.02 eV. These should be compared to the E_d for an isolated molecule, 2.12 eV. Thus, the

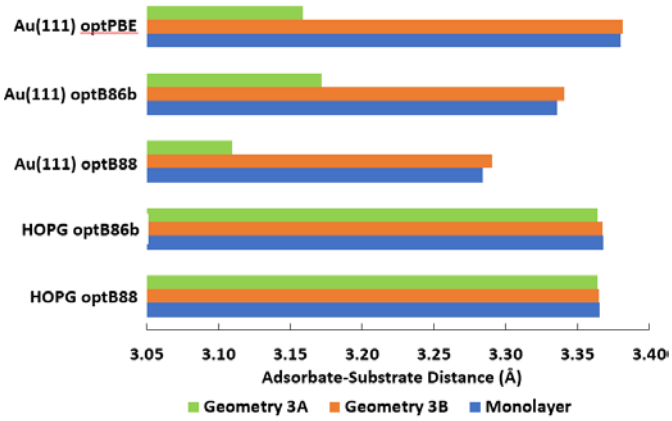

Figure 6. Average distance between coronene and substrate (HOPG or Au(111)) from DFT optimized structures with different functionals. The colored bars represent distances in Å for 3 geometries. Green: isolated molecule on substrate (Figure 3A), Orange: monolayer with one cavity (Figure 3B), Blue: complete monolayer (Figure 2).

desorption energy can vary by ~0.4 eV depending upon the coverage.

An interesting observation was made when we compare the coronene-substrate distances from DFT optimized geometries. Fig. 6 shows coronene-Au(111) and coronene-HOPG distances from three geometries shown in Fig. 2, 3A and 3B which represent the complete monolayer, isolated molecule and a monolayer with single cavity respectively. These geometries were chosen to illustrate the effect of surface coverage on the adsorption distances. From Fig. 6, we can see that surface coverage has negligible effect for coronene-HOPG distances (3.36 Å). This indicates that intermolecular interactions between the coronene adsorbates does not affect the surface binding on HOPG. Contrarily, the coronene-Au(111) distances vary considerably with surface coverage and cavities. For example, in DFT optimized geometries with optB88-vdW functional,[55,56] the coronene-Au(111) distance (Fig. 6) for an isolated molecule (Fig. 3A) is 3.11 Å, while it is 3.28 Å for a complete monolayer (Fig. 2) and 3.29 Å for the molecules in the immediate vicinity of a single cavity (Fig. 3B). From Fig. 6, we can see that the coronene monolayer moves up by ~0.2 Å relative to an isolated coronene molecule on a Au(111) substrate. This phenomenon can be attributed to cooperative binding in coronene-Au(111) system with variable surface coverage.

In this study, we could not fully establish the reason for cooperative behavior of Au(111) substrate (Fig. 6), but our previous study[9] of coronene on Au(111) showed that there is significant a charge redistribution at the interface upon the adsorption of coronene on Au(111). We think that charge redistribution may be one of the causes for cooperativity on Au substrate. Additionally, we also noticed adsorption cooperativity within the coronene-Au(111) geometry with a cavity (Fig. 3B). In this geometry, the adsorption distances vary mildly as you move away from the cavity. A detailed analysis of coronene adsorption distances in Geometry 3B (Fig. 3) is shown section S4 of supporting information. This phenomenon is consistent with our earlier observations of relatively higher error fluctuations, $F(a)_i$, in coronene/Au(111) systems (Fig. 4, 5) due to cooperativity.

Note that coronene molecules can vibrate, translate, and rotate on the substrate leading to further changes in the calculated desorption energy. Thrower et al. calculated[30] the electronic energies of rotation and translation of coronene on HOPG with DFT. Their work indicates that electronic energy component of rotational and translational energies for coronene on HOPG are in the order of 0 to 0.2 eV. Their study indicates that desorption of coronene molecules are affected by the translational and rotational energy components. However, a complete analysis requires consideration of nuclear motion in addition to electronic energies, which will be addressed in a forthcoming paper. Using all the data shown in Fig. 4, 5 and Tables 1, 2 we have shown that coronene molecule desorption exhibits coverage dependence. Thus, the simple model presented here may be useful for adsorbate-substrate systems exhibiting weak cooperativity but is less useful for systems with significant cooperativity.

Fig. 7 shows $F(a)_i$ values for each "coronene ML only" systems obtained from optB88 and optB86b vdW-DF functionals. The $F(a)_i$ values range within 20 meV for "coronene ML only" from both HOPG and Au(111) substrates with both

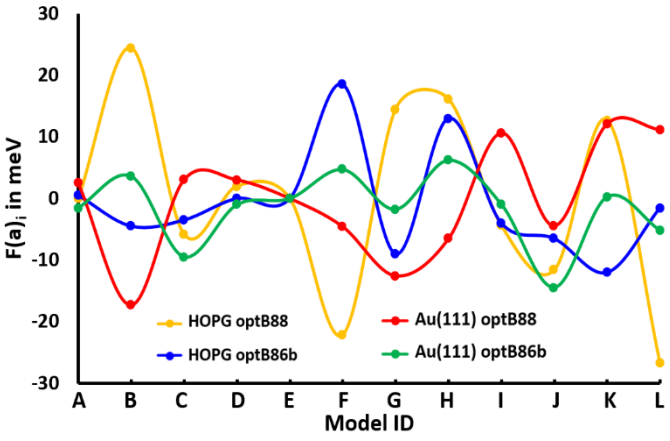

Figure 7. Errors, $F(a)_i$, in contact energy (in meV) for each geometry (see Figure 3) of coronene only layer (where, substrate removed = HOPG (orange, blue) or Gold (red, green)) with optB88 and optB86b vdW-DF functionals. The error fluctuation (y-axis) in each plot is relative to energy (E_0) of single isolated coronene molecule without the substrate. The line connecting points is solely meant to guide the eye.

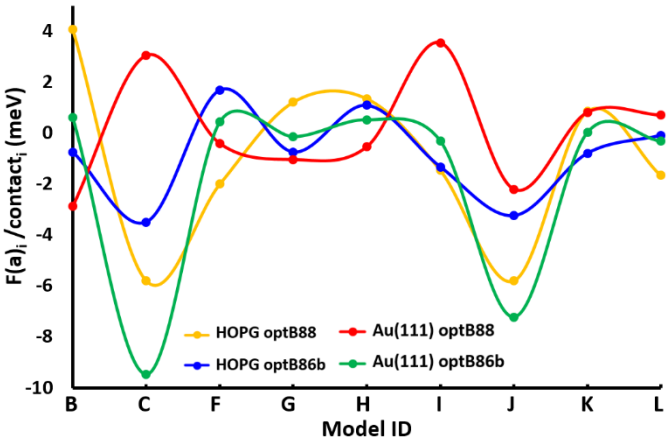

Figure 8. Errors per contact, $F(a)_i/c_i$, for geometries with contacts (see Figure 3) of coronene only layer (where, substrate removed = HOPG (orange, blue) or Gold (red, green)) with optB88 and optB86b vdW-DF functionals. The error fluctuation (y-axis) in each plot is relative to energy (E_0) of single isolated coronene molecule without the substrate. The line connecting points is solely meant to guide the eye.

DFT functionals. This indicates that regardless of the functional used the error in coronene-coronene contact energies is small compared to the coronene/substrate systems (Fig. 4). The error per contact is graphed in Fig. 8. For "coronene ML only" from both HOPG and Au(111) substrate geometries, the error fluctuation reduced from 20 meV (Fig. 4) to 10 meV (Fig. 5).

The average intermolecular contact energies, 'a' values, are determined to be 54 meV for "coronene ML only from HOPG", while 'a' = 40 meV for "coronene ML only from Au(111)" with both functionals. The higher 'a' for "coronene ML only" from HOPG (54 meV) than from Au(111) (40 meV) can be attributed to the denser coronene-coronene packing on HOPG substrate[49] (by ~0.28 Å) than on Au(111) substrate.[45] Comparison of coronene contact energies ('a') with and without the substrate (Table 2), we notice that 'a' values are similar for coronene with or without HOPG (~55 meV). This indicates that HOPG substrate plays little role in the intermolecular contact energies. On the other hand, 'a' values for coronene with or without Au(111) substrate vary significantly indicating again that gold substrate plays a significant role in the intermolecular contact energies. Hence, coronene contact energies exhibit substrate dependence on Au(111) and HOPG.

Conclusions

To summarize, we performed PW-DFT calculations with vdW-DF functionals on coronene/substrate (substrate = Au(111), HOPG) systems to determine coverage dependent desorption energies at the single molecule level. We showed that single molecule desorption in a physisorbed SAM is a complex process (Fig. 1) and dependent on the coverage and substrate. Using multiple geometries (Fig. 2, 3) developed based on predetermined experimental STM images of coronene SAM on Au(111) and HOPG, we calculated the electronic contributions to the single molecule desorption energies and intermolecular contact energies. The computational results were least squares fit (LSF) to a simple nearest neighbor model in order to account for intermolecular contact energies. Data (Fig. 4-8 and Tables 1 and 2) from PW-DFT calculations and LSF analysis indicates that coronene molecules have contact energies of about 54 meV with or without the HOPG substrate indicating little substrate dependence in the monolayer packing. On Au(111), coronene exhibited cooperative binding with variable surface coverage. The adsorption distances, desorption energies and intermolecular coronene-coronene contact energies varied considerably with various amounts of coverage (Fig. 2, 3) for the coronene/Au(111) system. This study presents a simple model to determine approximate position dependent desorption energies that, for systems showing weak adsorbate-substrate cooperativity, can be used with Monte Carlo simulations to predict accurate desorption versus coverage data. On the other hand, systems with significant cooperativity are not well reproduced by a nearest neighbor model. In fact, attempts to use a quadratic dependence on number of neighbors gave equally poor results in the coronene/Au(111) case.

Acknowledgements

We gratefully acknowledge support of this work by the US National Science Foundation (CHE-1800070). The computational work was performed using resources from the Center for Institutional Research Computing (CIRC) at Washington State University (WSU) and from EMSL (grant 48783), a DOE Office of Science User Facility located at Pacific Northwest National Laboratory (PNNL).

References

1 Ulman, *Chem. Rev.* 1996, **96**, 1533−1554.
2 J. C. Love, L. A. Estroff, J. K. Kriebel, R. G. Nuzzo and G. M. Whitesides, *Chem. Rev.* 2005, **105**, 1103–1170.
3 S. Casalini, C. A. Bortolotti, F. Leonardi and F. Biscarini, *Chem. Soc. Rev.* 2017, **46**, 40–71.
4 Schoenbaum, D. K. Schwartz and J. W. Medlin, *Acc. Chem. Res.* 2014, **47**, 1438–1445.
5 G. K. Jennings and P. E. Laibinis, *Colloids Surf., A* 1996, **116**, 105−114.
6 R. Y. Lai, D. S. Seferos, A. J. Heeger, G. C. Bazan and K. W. Plaxco, *Langmuir* 2006, **22**, 10796–10800.
7 U. Mazur and K. W. Hipps, *Chem. Commun.* 2015, *51*, 4737– 4749.
8 K. S. Mali, N. Pearce, S. De Feyter and N. R. Champness, *Chem. Soc. Rev.* 2017, **46**, 2520–2542.
9 Jahanbekam, B. Chilukuri, U. Mazur and K. W. Hipps, *J. Phys. Chem. C* 2015, **119**, 25364–25376.
10 G. Nandi, B. Chilukuri, K. W. Hipps and U. Mazur, *Phys. Chem. Chem. Phys.* 2016, **18**, 20819– 20829.
11 S. Whitelam, *Adv. Mater.* 2015, **27**, 5720– 5725.
12 R. Valiokas, M. Östblom, S. Svedhem, S. C. T. Svensson and B. J. Liedberg, *J. Phys. Chem. B* 2002, **106**, 10401–10409.
13 D. Lindstrom, M. Muntwiler and X. Y. Zhu, *J. Phys. Chem. B* 2007, **111**, 6913– 6920.
14 R. S. Smith and B. D. Kay, *J. Phys. Chem. B* 2018, **122**, 587– 594.
15 S. Karpovich and G. J. Blanchard, *Langmuir* 1994, **10**, 3315-3322.
16 G. Ghanizadeh and G. Asgari, *Reaction Kinetics, Mechanisms and Catalysis* 2011, **102**, 127-142.

17 H. M. Schessler, D. S. Karpovich and G. J. Blanchard, *Journal of the American Chemical Society* 1996, **118**, 9645-9651.
18 D. Bain, E. B. Troughton, Y.-T. Tao, J. Evall, G. M. Whitesides, and R. G. Nuzzo, *Journal of the American Chemical Society* 1989, **111**, 321-335.
19 Y. H. Yuan, C. M. Yam, O. E. Shmakova, R. Colorado Jr., M. Graupe, H. Fukushima, H. J. Moore and T. R. Lee, *J. Phys. Chem. C* 2011, **115**, 19749–19760.
20 L. S. Jung, C. T. Campbell, T. M. Chinowsky, M. N. Mar, and S. S. Yee, *Langmuir* 1998, **14**, 5636– 5648.
21 L. S. Jung and C. T. Campbell, *J. Phys. Chem. B* 2000, **104**, 11168-11178.
22 O. Dannenberger, M. Buck and M. Grunze, *Journal of Physical Chemistry B* 1999, **103**, 2202-2213.
23 R. Madueno, T. Pineda, J. M. Sevilla and M. Blazquez, *Journal of Electroanalytical Chemistry* 2005, **576**, 197–203.
24 T. J. Mullen, A. A. Dameron, H. M. Saavedra, M. E. Williams and P. S. Weiss, *Journal of Physical Chemistry C* 2007, **111**, 6740-6746.
25 S. Kundu, W. Xia, W. Busser, M. Becker, D. A. Schmidt, M. Havenith and M. Muhler, *Phys. Chem. Chem. Phys.* 2010, **12**, 4351–4359
26 H. Kang, Y. Kim, I. Choi, R. Chang and W. Yeo, *Analytica Chimica Acta*, 2014, **843**, 38–45.
27 L. S. Nieskens, A. P. van Bavel and J. W. Niemantsverdriet, *Surf. Sci.*, 2003, **546**, 159.
28 P. J. Barrie, *Phys. Chem. Chem. Phys.*, 2008, **10**, 1688.
29 W. Liu, F. Maaß, M. Willenbockel, C. Bronner, M. Schulze, S. Soubatch, F. S. Tautz, P. Tegeder and A. Tkatchenko , *Phys. Rev. Lett.*, 2015, **115** , 036104.
30 J. D. Thrower, E. E. Friis, A. L. Skov, L. Nilsson, M. Andersen, L. Ferrighi, B. Jorgensen, S. Baouche, R. Balog, B. Hammer and L. Hornekær, *J. Phys. Chem. C* 2013, **117**, 13520–13529.
31 J.W. Niemantsverdriet, P. Dolle, K. Markert, and K. Wandelt, *J. Vac. Sci. Technol. A* 1987, **5**, 875.
32 W. Song, N. Martsinovich, W. M. Heckl and M. Lackinger, J. *Am. Chem. Soc.* 2013, **135**, 14854–14862.
33 K. W. Hipps and A. Bhattrai, In *Encyclopedia of Interfacial Chemistry*; Wandelt, K. Eds.; Elsevier, 2018, 100-109, ISBN- 9780128098943. DOI: 10.1016/B978-0-12-409547-2.13048-3.
34 J. K. Nørskov, T. Bligaard, B. Hvolbaek, F. Abild-Pedersen, I. Chorkendorff and C. H. Christensen, *Chem. Soc. Rev.*, 2008, **37**, 2163–2171.
35 G. A. Samorjai and Y. Li, *Introduction to Surface Chemistry and catalysis 2nd Ed.*, John Wiley and Sons Inc., New Jersey, 2010.
36 J. K. Nørskov, F. Abild-Pedersen, F. Studt and T. Bligaard, *Proc. Natl. Acad. Sci. U. S. A.*, 2011, **108**, 937–943.
37 R. J. Maurer, V. G. Ruiz, J. Camarillo-Cisneros, W. Liu, N. Ferri, K. Reuter and A. Tkatchenko, *Prog. Surf. Sci.* 2016, **91**, 72–100.
38 P. Lazar, F. Karlicky, P. Jurečka, M. Kocman, E. Otyepkova, K. Šafářova and M. Otyepka *J. Am. Chem. Soc.* 2013, **135**, 6372– 6377
39 W. Liu, A. Tkatchenko and M. Scheffler, *Acc. Chem. Res.* 2014, **47**, 3369– 3377
40 Heimel, L. Romaner, J.-L. Brédas and E. Zojer, *Surf. Sci.* 2006, **600**, 4548– 4562.
41 Z. Hu, B. Li, A. Zhao, J. Yang and J. G. Hou, *J. Phys. Chem. C* 2008, **112**, 13650– 13655.
42 Terentjevs, M. P. Steele, M. L. Blumenfeld, N. Ilyas, L. L. Kelly, E. Fabiano, O. L. A. Monti and F. Della Sala, *J. Phys. Chem. C* 2011, **115**, 21128–21138.
43 Y. Chin, D. Panduwinata, M. Sintic, T. J. Sum, N. S. Hush, M. J. Crossley and J. R. Reimers, *J. Phys. Chem. Lett.* 2011, **2**, 62– 66.
44 Chilukuri and T. R. Cundari, *Surf. Sci.* 2012, **606**, 1100−1107.
45 Jahanbekam, S. Vorpahl, U. Mazur and K. W. Hipps, *J. Phys. Chem. C* 2013, **117**, 2914– 2919.
46 S. Uemura, M. Sakata, I. Taniguchi, C. Hirayama and M. Kunitake, *Thin Solid Films* 2002, **409**, 206– 210.
47 M. Yano, M. Endo, Y. Hasegawa, R. Okada, Y. Yamada and M. J. Sasaki, *Chem. Phys.* 2014, **141**, 034708.
48 F. Raigoza, D. A. Villalba, N. A. Kautz and S. A. Kandel, *Surf. Sci.* 2010, **604**, 1584–1590. (and references therein)
49 K. Walzer, M. Sternberg and M. Hietschold, *Surf. Sci.* 1998, **415**, 376–384.
50 Y. L. Yang, K. Deng, Q. D. Zeng and C. Wang, *Surf. Interface Anal.* 2006, **38**, 1039–1046.
51 G. Kresse, and J. Hafner, *Phys. Rev. B* 1993, **47**, 558-561.
52 G. Kresse and J. Furthmüller, *Phys. Rev. B* 1996, **54**, 11169.
53 G. Kresse and D. Joubert, *Phys. Rev. B* 1999, **59**, 1758.
54 P. E. Blöchl *Phys. Rev. B* 1994, **50**, 17953.
55 J. Klimeš, D. R. Bowler and A. Michaelides, *Phys. Rev. B* 2011, **83**, 195131.
56 M. Dion, H. Rydberg, E. Schroder, D. C. Langreth and B. I. Lundqvist, *Phys. Rev. Lett.*, 2004, **92**, 246401.
57 G. Li, I. Tamblyn, V. R. Cooper, H. -J. Gao and J. B. Neaton, *Phys. Rev. B: Condens. Matter Mater. Phys.* 2012, **85**, 121409.
58 V. G. Ruiz, W. Liu, E. Zojer, M. Scheffler and A. Tkatchenko, *Phys. Rev. Lett.* 2012, **108**, 146103.
59 B. Chilukuri, U. Mazur and K. W. Hipps *Phys. Chem. Chem. Phys.* 2014, **16** (27), 14096-14107.
60 H. J. Monkhorst and J. D. Pack, *Phys. Rev. B* 1976, **13**, 5188.
61 V. Talyzin, S. M. Luzan, L. Leifer, S. Akhtar, J. Fetzer, F. Cataldo, Y. O. Tsybin, C. V. Tai, A. Dzwilewski and E. Moons *J. Phys. Chem. C* 2011, **115**, 13207–13214
62 P. V. C. Medeiros, G. K. Gueorguiev and S. Stafström, *Phys. Rev. B: Condens. Matter Mater. Phys.* 2012, **85**, 205423
63 S. Gautier, S. N. Steinmann, C. Michel, P. Fleurat-Lessard and P. Sautet, *Phys. Chem. Chem. Phys.*, 2015, **17**, 28921.
64 W. Reckien, M. Eggers and T. Bredow, *Beilstein J. Org. Chem.* 2014, **10**, 1775–1784.
65 J. Hermann, R. A. DiStasio Jr and A. Tkatchenko, *Chem. Rev.*, 2017, **117**, 4714.
66 K. Berland, V. R. Cooper, K. Lee, E. Schröder, T. Thonhauser, P. Hyldgaard and B. I. Lundqvist, *Rep. Prog. Phys.* 2015, **78**, 66501.